JOURNAL OF CHEMICAL & ENGINEERING DATA

ARTICLE

pubs.acs.org/jced

Liquid−Liquid Phase Behavior of Solutions of 1-Butyl-3-methylimidazolium Bis((trifluoromethyl)sulfonyl)amide (C_4mimNTf_2) in *n*-Alkyl Alcohols

Vlad R. Vale,[†] Bernd Rathke,[*,†] Stefan Will,[†] and Wolffram Schröer[‡]

[†]Universität Bremen, Technische Thermodynamik, Badgasteiner Str. 1, 28359 Bremen, Germany

[‡]Universität Bremen, FB2, Institut für Anorganische und Physikalische Chemie, Leobener Str. NWII, 28359 Bremen, Germany

ABSTRACT: Liquid−liquid phase diagrams of binary mixtures of the ionic liquid 1-butyl-3-methylimidazolium bis((trifluoromethyl)sulfonyl)amide (C_4mimNTf_2) with *n*-alkyl alcohols (butan-1-ol, pentan-1-ol, hexan-1-ol, heptan-1-ol, octan-1-ol, nonan-1-ol, decan-1-ol, and undecan-1-ol) are reported. Phase diagrams were determined at atmospheric pressure over the temperature range (280 to 420) K using the cloud-point method. The phase behavior indicates partial miscibility, with upper critical solution temperatures (UCSTs) between (297 and 408) K. With increasing chain length of the alcohol, the UCST shifts toward higher temperatures and slightly higher concentrations. Ising criticality is presumed for the numerical analysis of the phase diagrams. The temperature dependence of the diameter of the phase diagram, which determines the asymmetry of the phase diagram, was analyzed presuming the validity of the rectilinear diameter rule of Cailletet-Mathias or, alternatively, a nonlinear shape as requested by the theory of complete scaling. The analysis yielded the UCST, the corresponding critical composition, and the width and diameter parameters that characterize the shape of the phase diagram. When the phase diagrams are represented in terms of corresponding states variables, the results for solutions of C_4mimNTf_2 and C_{12}mimNTf_2 become very similar.

INTRODUCTION

In this work, we further pursue the goal of a systematic characterization of a group of phase diagrams that belong to the family of solutions of ionic liquids (ILs) of the type 1-alkyl-3-methylimidazolium bis((trifluoromethyl)sulfonyl)amide ($C_x$mimNTf_2) in *n*-alkyl alcohols[1−3] to provide basic data for research and application. In this work, we consider solutions of 1-butyl-3-methylimidazolium bis((trifluoromethyl)sulfonyl)amide (C_4mimNTf_2). Former studies concerned the ILs $C_x$mimNTf_2 with x = 6, 8, 10, and 12.[1−3]

K. N. Marsh was among the first researchers to report studies of the liquid−liquid phase diagrams of alcohol solutions of room-temperature ILs containing the PF_6^- anion.[4,5] These investigations together with the work simultaneously performed by other groups[6−10] triggered the research on liquid−liquid phase diagrams of solution of ILs.[1−3,11−28] Before the discovery of ILs, the observation of phase diagrams of ionic solutions was a rather rare event.[29−35] Now, because of the chemical variability of ILs, systematic investigations of the relations between the phase diagram and the chemical structures of the components are feasible. They provide basic data for chemical engineering work (e.g., see ref 36) and the development of equations of state for solutions of ILs with relevance, e.g., for extractions[37] and two-phase reactions.[38]

While the interest in ILs with the anions BF_4^- and PF_6^- [4−9,11,12,14,39] has faded because those salts suffer from hydrolysis (e.g., see refs 40 and 41) and develop hazardous HF, the rather stable ILs with the NTf_2^- anion have attracted increasing interest.

Another reason for the particular interest in ILs containing NTf_2^- is that this anion is rather hydrophobic, causing some of these ILs to be soluble even in nonpolar solvents.[15,25−27] We are systematically studying the influence of the chain length of the alcohol and the side chains of the ILs on the thermodynamic properties of the IL solutions. Investigations of mixtures with alcohols are informative because varying the chain length of the alcohols changes not only the relative size of the components of the solution but also the dielectric permittivity and the volume ratio of the polar OH group to the nonpolar tail. In principle, such investigations can cover the range from highly polar to nonpolar solvents[6,12,17] (e.g., from water[6,9,12] to hydrocarbons[17,22,42]). Varying the length of the side chain of the cation not only changes the hydrophobicity of the IL but also causes structural changes. With increasing length of the side chain, the ILs show an increasing tendency for microscopic segregation of the salts into ionic and hydrophobic regions (e.g., see refs 43−46). For longer side chains (x > 10), liquid-crystalline domains are formed for salts with the anions Cl^-, Br^-, BF_4^-, and PF_6^-. This complication is avoided by considering ILs with NTf_2^-,[47] which is nonspherical and has different conformers,[48] thus reducing local ordering.

A reliable representation of thermodynamic data (e.g., phase diagrams) with a minimum number of parameters is useful and can be achieved on the basis of adequate models. In the vicinity of critical points (CPs) of both liquid−gas and liquid−liquid equilibria, including the upper critical solution point (UCSP) considered in this paper, phase transitions of nonionic systems show the same universal critical properties as the 3D Ising model.[49−51] The temperature dependence of the difference

Special Issue: Kenneth N. Marsh Festschrift

Received: July 28, 2011
Accepted: September 27, 2011
Published: October 20, 2011

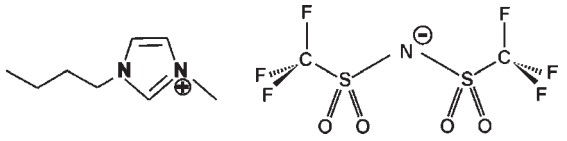

Figure 1. Structure of the ionic liquid 1-butyl-3-methylimidazolium bis((trifluoromethyl)sulfonyl)amide (C_4mimNTf$_2$).

between compositions in the coexisting phases is universally determined by the power law $|T - T_c|^{\beta}$, which depends on the separation of the transition temperature T from the critical temperature T_c of the phase transition considered. The exponent β takes up the universal value $\beta = 0.326$,[49−51] while all mean-field theories, including generalized van der Waals theories,[51] the theory of regular solutions,[51] and approaches based on the quasi-chemical approximation,[36] yield the value $\beta = 0.5$, in contrast to the experiments. Thus, empirical equations of state for describing the liquid−gas phase diagrams of organic compounds[52] provided in the Landolt−Börnstein tables edited by K. N. Marsh involve the universal value of β.

Ising criticality is generally expected when the phase transition is driven by short-range r^{-n} interactions with $n \geq 4.97$.[53] As explicated in our former reports,[1−3,30−33,39] ionic systems also show Ising behavior in spite of the long-range nature of the Coulomb interactions, which vary with r^{-1}. For reviews of the story of criticality in Coulomb systems, consider refs 54 and 55.

Ising critical behavior does not imply that the phase diagrams can be completely represented by the Ising model. While the phase diagram of the Ising model is symmetric, the phase diagrams of the liquid−gas and liquid−liquid phase transitions are in general asymmetric, which means that the average composition of the two phases, termed the diameter, varies with temperature. According to the recently developed theory of "complete scaling", the temperature dependence of the diameter is described by a power series in $|T - T_c|$ involving a linear term and nonanalytical terms[56−58] with the exponents $1 - \alpha$ and 2β, respectively. The term determined by the exponent 2β is the leading term in general.[59] We recall that $\alpha = 0.11$ is the critical exponent determining the divergence of the specific heat.[49−51,56−58] Thus, the linear temperature variation near the critical point, which is known as the rectilinear diameter rule of Cailletet-Mathias[51] and is predicted by the van der Waals equation[51] and other mean-field theories,[51,53] may not suffice as a Taylor expansion in powers of $|T - T_c|$ with natural numbers as exponents. An overview of complete scaling and further corrections due to the crossover from Ising to mean-field criticality and for the liquid−gas transition of one-component systems and the liquid−liquid transition in binary mixtures is provided in a recent review by Behnejad et al.[60]

In this paper, we report eight phase diagrams of mixtures of C_4mimNTf$_2$ (Figure 1) with *n*-alkyl alcohols (n = 4, 5, 6, 7, 8, 9, 10, 11) that supplement our previous reports on solutions of C_6mimNTf$_2$,[3] C_8mimNTf$_2$,[1] C_{10}mimNTf$_2$,[1] and C_{12}mimNTf$_2$.[2] A numerical data analysis was carried out in order to obtain the parameters characterizing the phase diagrams and allow for a quantitative assessment of the influence of the chain length of the alcohol on the location and shape of the phase diagram. For the data analysis, Ising criticality was presumed, and a linear term or a nonanalytical term with the exponent 2β was taken into account for modeling the diameter. The literature data for solutions in butan-1-ol,[11] hexan-1-ol,[11] and octan-1-ol[28] were also analyzed. A subsequent corresponding states analysis with the reduced variables $|T_c - T|/T_c$ and $(x - x_c)/x_c$, where x is the mole fraction of the IL and x_c is the mole fraction at the upper critical solution temperature (UCST) obtained by the preceding analysis, demonstrated that the phase diagrams in the scaled variables merge with each other almost perfectly. The corresponding state analysis showed remarkable agreement between the phase diagrams of C_4mimNTf$_2$ and C_{12}mimNTf$_2$.

EXPERIMENTAL SECTION

Materials. The *n*-alkyl alcohols butan-1-ol [C_4OH; $C_4H_{10}O$, CAS no. 71-36-3, mass-fraction purity $w \geq 0.997$; $\varepsilon(T = 298.15\ K) = 17.22$[61]], pentan-1-ol [$C_5$OH; $C_5H_{12}O$, CAS no. 71-41-0, mass-fraction purity $w \geq 0.99$; $\varepsilon(T = 298.15\ K) = 14.30$[61]], hexan-1-ol [$C_6$OH; $C_6H_{14}O$, CAS no. 111-27-3, mass-fraction purity $w \geq 0.991$; $\varepsilon(T = 298.15\ K) = 12.17$[61]], heptan-1-ol [$C_7$OH; $C_7H_{16}O$, CAS no. 111-70-6, mass-fraction purity $w \geq 0.998$; $\varepsilon(T = 298.15\ K) = 10.78$[61]], octan-1-ol [$C_8$OH; $C_8H_{18}O$, CAS no. 111-87-5, mass-fraction purity $w \geq 0.99$; $\varepsilon(T = 298.15\ K) = 9.60$[61]], nonan-1-ol [$C_9$OH; $C_9H_{20}O$, CAS no. 143-08-8, mass-fraction purity $w \geq 0.993$; $\varepsilon(T = 298.15\ K) = 8.18$[61]], decan-1-ol [$C_{10}$OH; $C_{10}H_{22}O$, CAS no. 112-30-1, mass-fraction purity $w \geq 0.998$; $\varepsilon(T = 298.15\ K) = 7.66$[61]], and undecan-1-ol [C_{11}OH; $C_{11}H_{24}O$, CAS no. 112-42-5, mass-fraction purity $w \geq 0.994$; $\varepsilon(T = 298.15\ K) = 6.74$[61]] were purchased from Merck ($C_{n=6,7,9,10,11}$OH; Merck KGaA, Darmstadt, Germany) or Sigma-Aldrich ($C_{n=4,5,8}$OH; Sigma-Aldrich Chemie GmbH, Steinheim, Germany) with the maximum purity available and were used after additional drying over molecular sieves but without further purification. The IL C_4mimNTf$_2$ ($C_{10}H_{15}F_6N_3O_4S_2$, CAS no. 174899-83-3, $w > 0.998$; halide < 100 ppm; water = 80 ppm) was purchased from IoLiTec (Ionic Liquids Technologies GmbH, Heilbronn, Germany) and degassed and dried before sample preparation. To remove the water and any volatiles, the C_4mimNTf$_2$ was filled into a 100 mL round-bottom flask (Schott Duran glass) under an inert argon atmosphere inside a glovebag (AtmosBag, Sigma-Aldrich) and dried under continuous stirring at a temperature of 338 K for about 24 h under a vacuum of $2 \cdot 10^{-5}$ bar. The drying process was frequently monitored by weighing the sample. We checked the mass loss of a sample of IL (typically containing 40 g) after the process of drying and found that the detectable loss of mass was less than 10^{-3} g within a period of 2 h.

Sample Preparation and Cloud Point Detection. The procedure for preparation of the samples and determination of cloud-point temperatures (T_{cloud}) using the synthetic method was similar to the one described in detail in the previous reports.[1−3] For the sake of clarity, we summarize here the important points in brief. Mixtures were prepared in Duran-glass tubes with a seal made of PTFE-coated silicon under a protective gas atmosphere (argon). The typical size of a sample was 1 g. The composition was determined gravimetrically with an accuracy of 10^{-3} g, which resulted in an overall uncertainty of the mole fraction (Δx_{IL}) of $\pm\ 10^{-3}$.

The transition temperatures defining the liquid−liquid phase diagrams of the IL + alcohol binary mixtures were determined by the cloud-point method in a water or oil bath using a Pt-100 sensor (uncertainty of calibration = ± 0.05 K) with an expanded uncertainty ($k = 2$) of $\Delta T = \pm\ 0.75$ K.

The T_{cloud} values were determined visually as the onset of the phase transition. As described elsewhere,[1−3] the combination of stepwise changes in the temperature together with a repeated homogenization of the samples and repeated iteration of the

Table 1. Data Set for the Liquid−Liquid Phase Diagrams of C_4mimNTf$_2$ + *n*-Alkyl Alcohol (C_nOH) Mixtures: Mass Fractions (w), Mole Fractions (x_{IL}), and Cloud-Point Temperatures (T_{cloud}) and Their Repeatabilities (δT)[a]

w	x_{IL}	T_{cloud}/K	δT/K
	C_4mimNTf$_2$ + Butan-1-ol		
0.149	0.030	289.91	0.05
0.231	0.051	294.51	0.05
0.329	0.080	296.39	0.05
0.387	0.100	296.72	0.05
0.456	0.129	296.79	0.05
0.502	0.151	296.79	0.05
0.585	0.199	296.22	0.05
0.657	0.253	294.80	0.05
0.707	0.299	291.85	0.05
0.754	0.351	288.71	0.05
0.791	0.399	284.51	0.05
0.824	0.452	279.88	0.05
	C_4mimNTf$_2$ + Pentan-1-ol		
0.291	0.080	314.76	0.08
0.345	0.100	315.28	0.05
0.412	0.129	315.54	0.06
0.458	0.151	315.54	0.07
0.541	0.200	315.28	0.05
0.614	0.251	314.46	0.07
0.669	0.299	312.35	0.05
0.720	0.351	309.79	0.06
0.760	0.398	306.05	0.05
0.798	0.453	301.76	0.06
	C_4mimNTf$_2$ + Hexan-1-ol		
0.113	0.030	323.45	0.05
0.181	0.051	329.00	0.05
0.264	0.080	331.79	0.06
0.316	0.101	332.32	0.05
0.381	0.130	332.37	0.11
0.426	0.153	332.60	0.05
0.510	0.202	332.31	0.06
0.587	0.258	331.55	0.05
0.636	0.299	330.28	0.07
0.695	0.357	327.34	0.05
0.734	0.402	324.36	0.06
0.778	0.460	320.59	0.08
	C_4mimNTf$_2$ + Heptan-1-ol		
0.101	0.030	337.27	0.05
0.165	0.052	342.99	0.05
0.239	0.080	345.79	0.05
0.292	0.103	346.71	0.05
0.350	0.130	347.18	0.05
0.399	0.155	347.38	0.05
0.475	0.201	347.29	0.06
0.549	0.253	346.93	0.06
0.605	0.298	345.86	0.05
0.672	0.363	343.40	0.08
0.706	0.400	341.29	0.06
0.751	0.455	337.77	0.05
	C_4mimNTf$_2$ + Octan-1-ol		
0.091	0.030	351.51	0.05
0.150	0.052	357.46	0.05
0.219	0.080	360.32	0.05
0.275	0.105	361.50	0.05
0.325	0.130	361.86	0.07
0.371	0.155	362.02	0.05
0.448	0.202	361.84	0.06
0.525	0.255	361.60	0.05
0.582	0.302	360.36	0.06
0.640	0.356	358.72	0.09
0.682	0.400	356.51	0.05
0.735	0.463	352.62	0.05
	C_4mimNTf$_2$ + Nonan-1-ol		
0.082	0.030	363.80	0.06
0.133	0.050	368.02	0.05
0.201	0.080	372.25	0.05
0.245	0.100	373.24	0.05
0.302	0.130	374.13	0.05
0.338	0.150	374.32	0.05
0.419	0.199	374.79	0.05
0.490	0.249	374.23	0.07
0.661	0.408	369.94	0.05
0.699	0.445	366.68	0.05
	C_4mimNTf$_2$ + Decan-1-ol		
0.076	0.026	377.12	0.05
0.122	0.050	384.44	0.05
0.188	0.080	388.10	0.05
0.226	0.010	389.01	0.05
0.269	0.122	389.79	0.05
0.396	0.198	390.31	0.05
0.467	0.249	389.93	0.05
0.531	0.299	390.10	0.05
0.585	0.347	387.35	0.05
0.635	0.396	384.30	0.05
0.687	0.453	381.96	0.05
	C_4mimNTf$_2$ + Undecan-1-ol		
0.174	0.080	401.45	0.10
0.214	0.100	403.71	0.06
0.266	0.129	406.17	0.05
0.303	0.152	406.28	0.05
0.376	0.199	408.57	0.05
0.449	0.251	407.54	0.06
0.510	0.300	406.65	0.05
0.568	0.351	403.24	0.05
0.617	0.400	401.20	0.05

[a] The expanded uncertainty ($k = 2$) in T_{cloud} was $\Delta T = \pm 0.75$ K. The uncertainty in x_{IL} ($\Delta x_{IL} = \pm 10^{-3}$) is due to the accuracy of the weight measurement and the sample size.

dx.doi.org/10.1021/je200792v |*J. Chem. Eng. Data* 2011, 56, 4829–4839

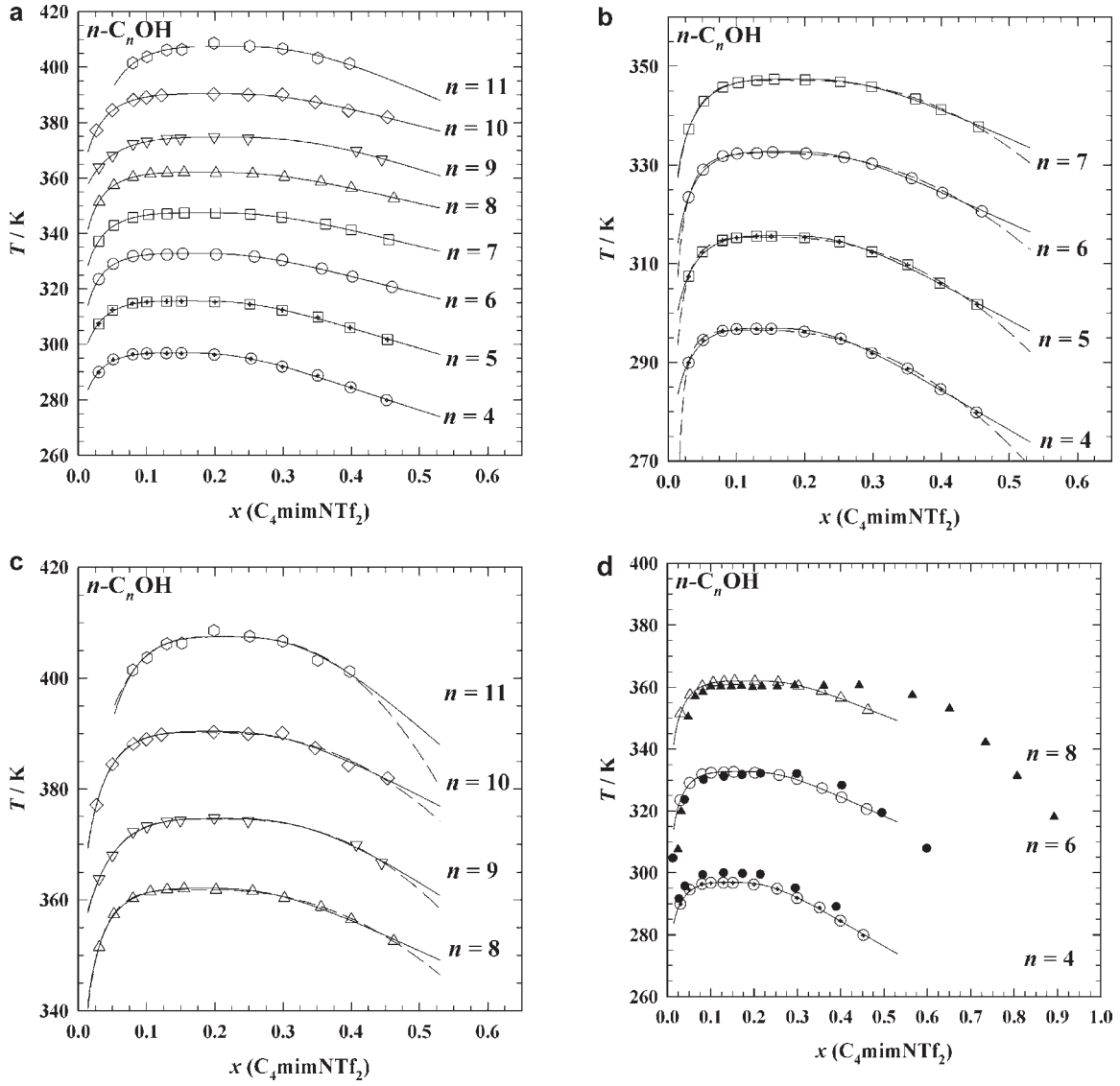

Figure 2. Isobaric phase diagrams at ambient pressure for C_4mimNTf$_2$ mixtures with *n*-alkyl alcohols (C_nOH). (a) Overview: ○ with cross, $n = 4$; □ with cross, $n = 5$; ○, $n = 6$; □, $n = 7$; △, $n = 8$; ▽, $n = 9$; ◇, $n = 10$; ⬡, $n = 11$. (b) Closer view: ○ with cross, $n = 4$; □ with cross, $n = 5$; ○, $n = 6$; □, $n = 7$. (c) Closer view: △, $n = 8$; ▽, $n = 9$; ◇, $n = 10$; ⬡, $n = 11$. (d) Comparisons with literature values: $n = 4$ (○ with cross, this work; ●, ref 11); $n = 6$ (○, this work; ●, ref 11); $n = 8$ (△, this work; ▲, ref 28). The concentration variable is the mole fraction of C_4mimNTf$_2$ ($x_{C_4\text{mimNTf}_2}$). The uncertainties in T and $x_{C_4\text{mimNTf}_2}$ are not visible in the resolution of the plot. The lines were obtained by fits of the experimental data: solid lines, eq 3; dashed lines, eq 4. The fit parameters are shown in Table 2.

T_{cloud} values results in the repeatabilities of T_{cloud} (δT) given in Table 1. The uncertainties were estimated from the accuracy of the T measurement and the repeatabilities of the observed transition temperatures. The influence of uncontrollable traces of impurities of the substances, which might affect the results in a systematic way, was not taken into account. However, checks on different batches of the substances used in this study showed no significant variations. Together with the statistical error, this effect results in a slight scatter of the T_{cloud} data, which can be estimated using the standard deviation of the fits from the experimental data.

■ RESULTS AND DISCUSSION

Experimental Results. The data for the phase diagrams are listed in Table 1. We give the mass fractions (w), the IL mole fractions (x_{IL}), the cloud-point temperatures (T_{cloud}), and the repeatabilities of the T_{cloud} determinations (δT) for solutions of C_4mimNTf$_2$ in the *n*-alkyl alcohols butan-1-ol, pentan-1-ol, hexan-1-ol, heptan-1-ol, octan-1-ol, nonan-1-ol, decan-1-ol, and undecan-1-ol.

The resulting phase diagrams are shown in Figure 2a−c, with the mole fraction of C_4mimNTf$_2$ as the composition variable. Figure 2a provides an overview of all of the phase diagrams for the mixtures of C_4mimNTf$_2$ with *n*-alkyl alcohols determined in this work, and Figure 2b,c allows for a closer look at the phase diagrams for the alcohols C_4OH, C_5OH, C_6OH, and C_7OH (Figure 2b) and C_8OH, C_9OH, C_{10}OH, and C_{11}OH (Figure 2c). Figure 2d shows a direct comparison of our data and the literature data for solutions in C_4OH,[11] C_6OH,[11] and C_8OH[28] (solid symbols).

The phase diagrams for all of the binary mixtures investigated are rather asymmetric and have a UCST. The binodals are steep at small concentrations of the salt and decay smoothly at compositions above the critical mole fraction x_c. The critical

dx.doi.org/10.1021/je200792v | J. Chem. Eng. Data 2011, 56, 4829–4839

Table 2. Parameters of the Liquid−Liquid Phase Diagrams of Solutions of the Ionic Liquid C_4mimNTf_2 in *n*-Alkyl Alcohols Obtained by Fitting the Experimental Curves with Equation 3 or 4 Using the Mole Fraction as the Composition Variable: Critical Temperatures (UCST; T_c), Critical Mole Fractions (x_c), Widths of the Coexistence Curves (B), and Values of the Parameters A and C That Determine the Diameter Are Given, along with Their Asymptotic Standard Errors Provided by the Fitting Routine and the Standard Deviation (σ) of the Residuals; B^*, C^* and σ^* Are the Coefficients and Standard Deviations of the Residuals Obtained by Fitting the Phase Diagrams Represented in Terms of the Corresponding State Variables

solvent	eq	T_c/K	x_c	$B/K^{-1/3}$	A/K^{-1}	$C/K^{-2/3}$	σ/K	B^*	A^*	C^*	$10^4 \cdot \sigma^*$
C_4OH	3	296.95 ± 0.14	0.145 ± 0.003	0.074 ± 0.001	0.0047 ± 0.0002	–	0.33	3.41 ± 0.06	9.52 ± 0.40	–	11.3
	4	296.56 ± 0.16	0.119 ± 0.006	0.081 ± 0.001	–	0.0199 ± 0.0016	0.42	4.56 ± 0.06	–	7.47 ± 0.61	14.3
C_4OH[a]	3	300.08 ± 0. 13	0.139 ± 0.003	0.072 ± 0.001	0.0056 ± 0.0003	–	0.26	3.49 ± 0.06	11.98 ± 0.64	–	8.6
	4	299.78 ± 0.28	0.129 ± 0.008	0.082 ± 0.002	–	0.0165 ± 0.0024	0.59	4.23 ± 0.08	–	5.73 ± 0.81	19.8
C_5OH	3	315.72 ± 0.13	0.159 ± 0.003	0.081 ± 0.001	0.0051 ± 0.0003	–	0.32	3.46 ± 0.05	10.12 ± 0.53	–	10.1
	4	315.38 ± 0.10	0.140 ± 0.003	0.089 ± 0.001	–	0.0180 ± 0.0010	0.27	4.30 ± 0.03	–	5.93 ± 0.32	8.4
C_6OH	3	332.74 ± 0.11	0.164 ± 0.003	0.084 ± 0.001	0.0060 ± 0.0003	–	0.28	3.54 ± 0.04	12.25 ± 0.58	–	8.5
	4	332.40 ± 0.11	0.148 ± 0.004	0.093 ± 0.001	–	0.0191 ± 0.0011	0.30	4.37 ± 0.03	–	6.22 ± 0.36	8.9
C_6OH[a]	3	333.01 ± 0.74	0.202 ± 0.011	0.088 ± 0.003	0.0041 ± 0.0005	–	1.70	3.03 ± 0.10	6.78 ± 0.89	–	51.1
	4	332.24 ± 0.37	0.181 ± 0.006	0.100 ± 0.001	–	0.0162 ± 0.0010	0.87	3.82 ± 0.04	–	4.31 ± 0.27	26.1
C_7OH	3	347.45 ± 0.07	0.181 ± 0.002	0.092 ± 0.001	0.0063 ± 0.0003	–	0.18	3.56 ± 0.03	12.09 ± 0.51	–	5.3
	4	347.23 ± 0.05	0.169 ± 0.002	0.099 ± 0.001	–	0.0170 ± 0.0005	0.13	4.12 ± 0.02	–	4.98 ± 0.15	3.9
C_8OH	3	362.09 ± 0.09	0.183 ± 0.002	0.093 ± 0.001	0.0067 ± 0.0003	–	0.23	3.63 ± 0.03	13.37 ± 0.66	–	6.3
	4	361.87 ± 0.06	0.171 ± 0.002	0.101 ± 0.001	–	0.0180 ± 0.0006	0.15	4.22 ± 0.02	–	5.35 ± 0.16	4.0
C_8OH[b]	3	363.52 ± 1.61	0.235 ± 0.018	0.096 ± 0.005	0.0055 ± 0.0007	–	5.14	2.94 ± 0.16	8.53 ± 1.15	–	14.2
	4	362.37 ± 0.98	0.227 ± 0.009	0.121 ± 0.003	–	0.0222 ± 0.0016	3.25	3.81 ± 0.08	–	4.97 ± 0.35	89.7
C_9OH	3	374.69 ± 0.19	0.207 ± 0.005	0.098 ± 0.001	0.0047 ± 0.0008	–	0.38	3.42 ± 0.04	8.48 ± 1.41	–	10.0
	4	374.60 ± 0.15	0.198 ± 0.004	0.102 ± 0.001	–	0.0119 ± 0.0013	0.29	3.70 ± 0.04	–	3.13 ± 0.33	7.7
$C_{10}OH$	3	390.37 ± 0.20	0.192 ± 0.005	0.094 ± 0.002	0.0059 ± 0.0006	–	0.47	3.58 ± 0.06	12.09 ± 1.29	–	11.9
	4	390.16 ± 0.26	0.182 ± 0.006	0.101 ± 0.002	–	0.0155 ± 0.0019	0.59	4.03 ± 0.08	–	4.53 ± 0.54	15.0
$C_{11}OH$	3	407.47 ± 0.37	0.214 ± 0.011	0.083 ± 0.003	0.0035 ± 0.0020	–	0.77	2.88 ± 0.12	6.66 ± 3.74	–	19.1
	4	407.42 ± 0.40	0.212 ± 0.015	0.085 ± 0.003	–	0.0070 ± 0.0050	0.83	2.97 ± 0.11	–	1.82 ± 1.31	20.5

[a] Data from ref 11. [b] Data from ref 28.

dx.doi.org/10.1021/je200792v | J. Chem. Eng. Data 2011, 56, 4829–4839

composition, which in binary mixtures agrees with the maximum temperature of the phase diagrams, is located at low concentrations, in the mole fraction range $0.1 < x_{IL} < 0.2$. Figure 2d includes the data from measurements on solutions in C_4OH,[11] C_6OH,[11] and C_8OH[28] taken from the literature. While our data for butan-1-ol and hexan-1-ol agree very well with those from the literature, the deviation in the case of octan-1-ol solutions is larger. The literature data for the octan-1-ol solutions, which cover a much larger composition and temperature range than shown in the figure, report for the top of the phase diagram a phase separation at noticeably lower temperature than our measurements; these data show a wider immiscibility region than our measurements and a trend of a double maximum (on the order of or, respectively, slightly above the uncertainty given there), indicating the possible presence of a third component.

The UCST increases with the chain length of the alcohol. This is a general observation that is expected from considerations of polarity and in agreement with observations on other solutions of ILs.[1−3,11,13,19−21] Reducing the dielectric permittivity of the solvent by increasing the chain length of the alcohol reduces the stability of the ionic solution, increasing the separation temperature. Analogously, increasing the length of the side chain of the cation enhances the hydrophobicity of the IL and thus the solubility in weakly polar organic solvents, which corresponds to a decrease in the separation temperature. These trends are well-known[4−15,17] and were pointed out previously by K. N. Marsh in connection with experiments on alcohol solutions of ILs with the PF_6^- anion.[4,5] Thus, phase separation with an UCST near ambient temperature was observable for solutions of C_{12}mimNTf$_2$ in *n*-alkyl alcohols with $n = 10$ to 20,[2] solutions of C_8mimNTf$_2$ and C_{10}mimNTf$_2$ in *n*-alkyl alcohols with $n = 8$ to 20,[1] solutions of C_6mimNTf$_2$ in *n*-alkyl alcohols with $n = 6$ to 14,[3] and solutions of C_4mimNTf$_2$ in *n*-alkyl alcohols with $n = 4$ to 11. Measurements on solutions with larger or smaller chain lengths of the alcohol were outside the temperature range accessible with present equipment.

The curves drawn in Figure 2a−c are fits based on eqs 3 (solid lines) and eq 4 (dashed lines), which will be introduced and explained in the next section. A difference between the fits is not noticeable on the scale of Figure 2a. Even for the more detailed representations in Figure 2b,c, the difference between the two fits is not noticeable for the temperature region investigated but would be expected to become relevant at higher concentrations of the salt, which were not investigated in this work.

A more detailed discussion of the phase diagrams requires a numerical analysis because the maxima are difficult to determine as the tops of the curves are very flat and the shapes of the curves appear rather similar for all of the systems. In the next section, we will discuss the results of the numerical analysis, which yielded the critical data and the parameters describing the shape of the phase diagrams.

Shape Analysis of the Coexistence Curves. To allow for a quantitative assessment, the phase diagrams were analyzed by fitting the data to equations that have been derived on the basis of the scaling laws used in the field of critical phenomena.[49−51] The steps that led to the working equations were explained in detail in former work.[2,26] For convenience, we give here only the working equations with a short explanation of the background. For liquid−liquid phase transitions of binary solutions, the so-called Wegner expansion describes the temperature dependence of the mole fractions x_+ and x_- in the two phases and of the so-called diameter $x_m = (x_+ + x_-)/2$ as power series in $T_c - T$, where T_c is the UCST. Some contributions that are expected to be small were neglected because of the rather small temperature range of (10 to 15) K investigated in this work. The linear term and the term with the exponent $1 - \alpha$ contributing to the temperature dependence of the diameter were treated as a single linear term, because those two terms could hardly be separated in the fitting procedure. The resulting simplified scaling laws are

$$x_\pm - x_m = \pm B\cdot(T_c - T)^\beta \quad (1)$$

where B is the width of the coexistence curve and

$$x_m = x_c + A\cdot(T_c - T) + C\cdot(T_c - T)^{2\beta} \quad (2)$$

in which A and C are constant parameters. We approximated the critical exponent as $\beta = {}^1/_3$, as used by Guggenheim[62] and in the Landolt−Börnstein tables edited by K. N. Marsh.[52] The value $\beta = {}^1/_3$ is close to the Ising value $\beta = 0.326$[49−51] and more convenient for the numerical analysis. Expanding $|x - x_m|^3$ to first order in A and C, solving for T, and expressing $T_c - T$ in x_m by the asymptotic power law yields T as a function of x. Presuming either a linear temperature dependence of the diameter in eq 2 (determined by the coefficient A) or the 2β term (with the coefficient C) as the only term determining the asymmetry of the phase diagram, we get the remarkably simple working equations given by eqs 3 and 4, respectively:

$$T = T_c - \frac{|x - x_c|^3}{B^3 \pm 3A\cdot|x - x_c|^2} \quad (3)$$

$$T = T_c - \frac{|x - x_c|^3}{B^3 \pm 3\cdot C\cdot B|x - x_c|} \quad (4)$$

The positive and negative signs correspond to the ranges $x < x_c$ and $x > x_c$, respectively. Thus, Ising criticality and the asymmetry of the phase diagrams are taken into account in a manner convenient for a fitting procedure. An equation that includes both of the coefficients A and C did not yield stable fits.

The results of those fits are given in Table 2 together with the asymptotic standard errors (ASEs) provided by the fitting routine for all quantities and the standard deviations σ of the fit residuals. The residuals of the fits with eqs 3 and 4 are shown in Figure 3a,b, respectively.

A difference in the quality of the two fits for the solutions of the C_4mimNTf$_2$ is not evident in the figures. The mean-square deviations of the fits of the different systems, shown in Table 2, also do not show a systematic difference between the fits with eq 3 and eq 4, which is in contrast to the analysis of the data obtained for ILs with larger side chains,[2] where the fits with eq 3 were moderately better. The averaged standard deviations for the fits of our data are $\sigma = 0.37$ for both equations. For the fits to the literature data for the mixtures with C_6OH and C_8OH, the standard deviations are much larger than for our data. For these cases, the fits with eq 4 are better than those with eq 3.

We now discuss how the parameters T_c, x_c, B, A, and C obtained from the fits vary with the chain length of the *n*-alkyl alcohol. Table 2 shows that with the exception of the critical temperature T_c, all of other variables (i.e., the critical mole fraction x_c, the width parameter B, and the parameters A and C determining the diameter) do not vary much with the chain length of the alcohol.

Figure 4a shows the critical temperature T_c as function of the chain length of the alcohol. As for the alcohol solutions of ILs

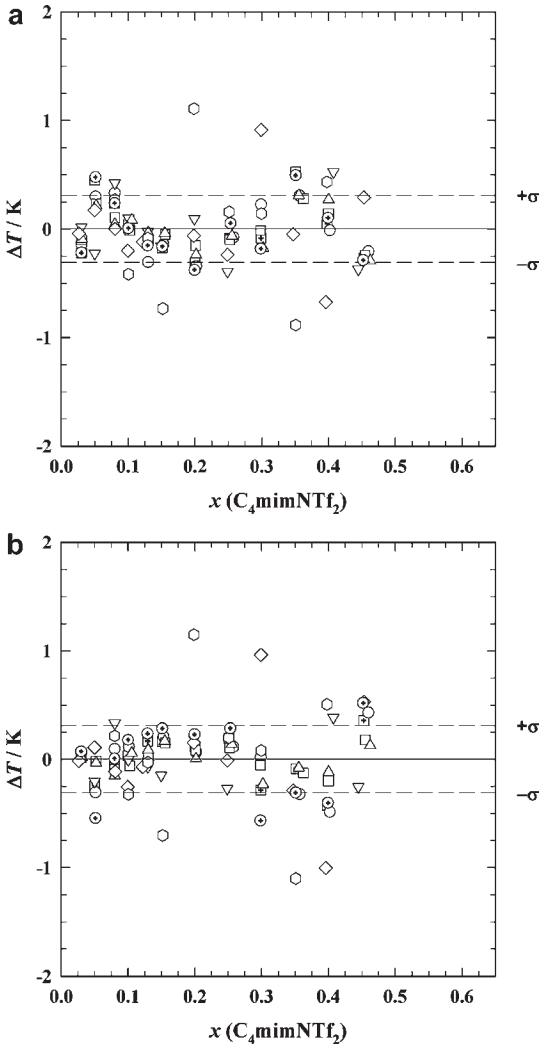

Figure 3. Deviations of the fitting results ($\Delta T = T_{fit} - T_{exptl}$) for the investigated systems using (a) eq 3 and (b) eq 4. The overall standard deviations σ are marked; the symbols denote the same *n*-alkyl alcohols (C_nOH) as in Figure 2 [○ with cross, $n = 4$; □ with cross, $n = 5$; ○, $n = 6$; □, $n = 7$; △, $n = 8$; ▽, $n = 9$; ◇, $n = 10$; ⬡, $n = 11$].

with longer side chains, we see an almost linear dependence of T_c on the chain length of the alcohol. The squares are the results obtained by fitting with eq 3, and the circles represent the results obtained by fitting with eq 4. Comparing the numerical analysis data in Table 2, we see that the analysis using eq 4 yields somewhat higher figures, although the differences are essentially within the ASE estimated for the fit. The ASE figures are too small to be seen on the scale of this plot. The figure includes the results obtained from the analysis of the data on solutions in butan-1-ol,[11] hexan-1-ol,[11] and octan-1-ol[28] reported by other groups. The solid symbols are the results for the data reported in this work, while the open symbols are based on the data reported by others. There are also no noticeable differences between our measurements and those from the literature. The symbols have been kept the same in the other panels in Figure 4 showing the values for the other parameters.

Figure 4b shows the critical mole fraction x_c as a function of the chain length of the alcohol. As for the critical temperature, we have included the results obtained by evaluating the data

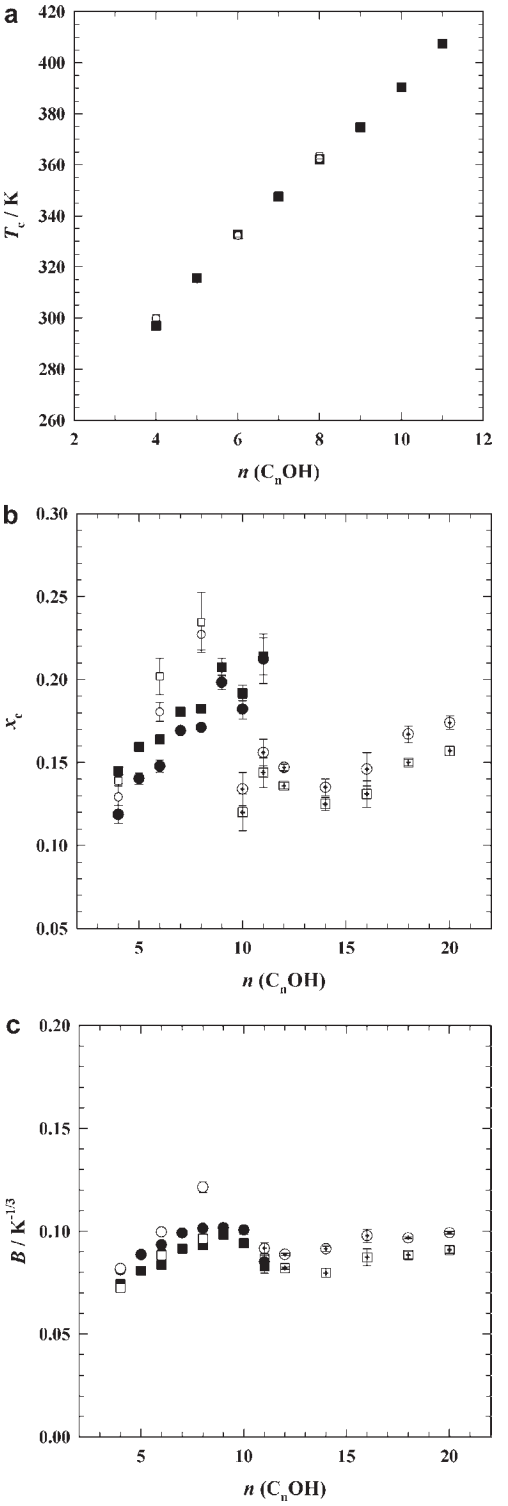

Figure 4. Representations of the characteristics of the phase diagrams for C_4mimNTf$_2$ + *n*-alkyl alcohol mixtures obtained by fitting with eq 3 (squares) and eq 4 (circles) as functions of the chain length *n* of the *n*-alkyl alcohols C_nOH: (a) critical temperature, T_c; (b) critical mole fraction, x_c; (c) width of the coexistence region of the phase diagram, *B*. The uncertainties in T_c and the differences between the results of the two methods are not visible in the resolution of the plot. The results of the present study are marked by solid symbols, data for C_{12}mimNTf$_2$[2] by open symbols with crosses, and other literature data[11,28] by open symbols.

dx.doi.org/10.1021/je200792v |*J. Chem. Eng. Data* 2011, 56, 4829–4839

reported in the literature. The figure also includes the results obtained for the mixture with the IL C_{12}mimNTf$_2$,[2] which is the IL with the longest side chain investigated to date. For the solutions of C_4mimNTf$_2$, the critical mole fractions increase almost linearly with the chain length of the alcohol. A minute modulation is noticeable that indicates a smaller value for alcohols whose chain length is an even number. For the solutions of C_{12}mimNTf$_2$, the critical mole fraction varies much less. It shows a slight minimum and is close to the figure for the solutions of C_4mimNTf$_2$ with butan-1-ol. The data for the solution of C_{10}OH in C_{12}mimNTf$_2$ are much less accurate than the other data, but we show them for the sake of completeness. The estimates of x_c obtained by evaluating the literature data for the solutions of C_6OH and C_4OH are larger than those obtained from the analysis of our data. As observed before,[2,3] the results for the critical composition obtained by the two fit methods are slightly different: the fits assuming the validity of the rectilinear diameter rule yield values for x_c that are always about 0.01 higher than those obtained from the fits taking only the 2β term into account. The bend of the nonlinear diameter in eq 4 leads to a smaller figure for the estimate of the critical mole fraction than the fit with eq 3. This deviation is larger than the ASE value obtained for the fits. In the preceding publications,[2,3] comparisons of the estimates of the critical compositions x_c with the values obtained by determining the critical mole fraction experimentally applying the equal volume criterion, together with the generally better fits obtained using eq 4, led us to the conclusion that fits with eq 4 are generally superior to those using eq 3. Here the fits of the data of the solutions of C_4mimNTf$_2$ do not yield systematically better fits with eq 4. The values of the standard deviation as well as the ASE values for the fits with eq 4, which approximates the diameter using the 2β term, are not smaller than those obtained in the fits using eq 3, which is based on the rectilinear diameter rule.

Figure 4c shows a trend for the width B similar to that found for x_c. Although the lengths of the side chains are rather different, we see very similar B values for the solutions of C_4mimNTf$_2$ and C_{12}mimNTf$_2$. For the solutions of C_4mimNTf$_2$, we see an increase with the chain length of the alcohol with a maximum for the nonan-1-ol solution, while for the solutions of C_{12}mimNTf$_2$, a slight minimum is observed near tetradecan-1-ol. The widths obtained using eq 4 come out larger than those obtained using eq 3.

While T_c, x_c, and B vary quite systematically with the chain length of the alcohol, the trends for the parameters A and C obtained by fitting with eqs 3 and 4, respectively, are more difficult to discuss. Again the figures obtained for the solutions of C_{12}mimNTf$_2$ and C_4mimNTf$_2$ are in the same region. While the values for the parameter A seem to indicate a maximum for both groups of systems, the values of C for the C_4mimNTf$_2$ solutions decrease with the chain length of the alcohol.

Corresponding State Analysis of the Phase Diagrams. In view of the large number of new systems, a data reduction by applying the concept of corresponding states is appropriate. As pointed out elsewhere[3,62,63] this concept is an ideal tool for the universal description of phase transitions. The theorem of corresponding states implies that scaling the thermodynamic variables by their critical data leads to a universal representation of the thermodynamic properties (e.g., of the phase diagrams). The phase diagrams match on a single master curve when represented in terms of variables that are scaled in such a manner. This has also been observed for solutions of ILs.[9,17,23,26,39,63,64]

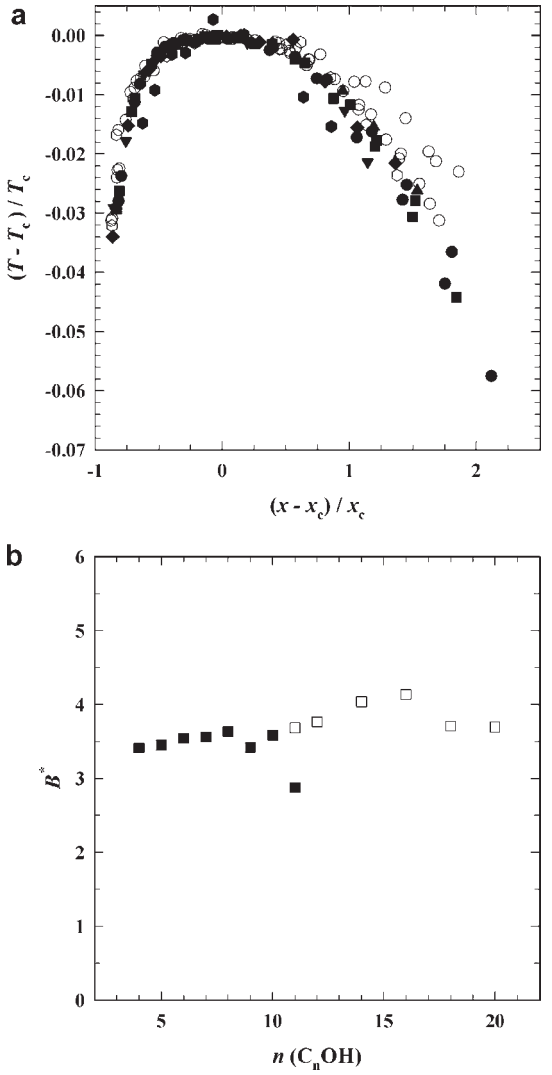

Figure 5. (a) Master plot of the phase diagrams of the solutions of C_4mimNTf$_2$ in alcohols (solid symbols) and C_{12}mimNTf$_2$ in alcohols (○).[2] Because all of the curves merge almost perfectly, they form an undistinguishable cloud of data points, where the symbols denote in principle the same *n*-alkyl alcohols (C_nOH) as in Figure 2. (b) Width of the coexistence region B^* of the phase diagram as obtained using eq 3; the results of the present study are marked by solid symbols and data for C_{12}mimNTf$_2$[2] by open symbols.

In Figure 5a we see a master plot of the phase diagrams of the solutions of C_4mimNTf$_2$ and C_{12}mimNTf$_2$ in alcohols obtained using the critical data taken from fits with eq 3. The reduced quantities for temperature and mole fraction are $|T_c - T|/T_c$ and $(x - x_c)/x_c$, respectively. The very reasonable representation of the phase diagrams of the solutions of both C_4mimNTf$_2$ and C_{12}mimNTf$_2$ in alcohols is remarkable not only because of the rather big differences in the molecular shapes of the two ILs and their solvophobic properties but also because of the large range of size, shape, and dielectric permittivity of the solvents. Figure 5b shows that the width parameter B^* in the corresponding states representation becomes almost constant, leading to the conclusion that the width B of the phase diagrams is a linear function of the critical mole fraction x_c. For the parameter A^* determining the diameter, no systematic trend can be identified. It is the

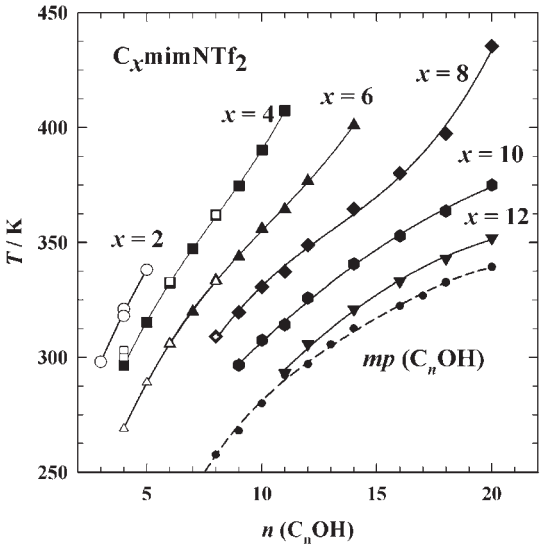

Figure 6. Dependence of the UCST on the chain length of C_nOH for different $C_x$mimNTf$_2$: ○, $x = 2$; □, $x = 4$ (this work); △, $x = 6$; ◇, $x = 8$; ⬡, $x = 10$; ▽, $x = 12$. Data from this and previous work[1−3] are denoted by solid symbols and data from the literature[10,11,14,20,28] by open symbols. The melting temperatures of the alcohols[65] are also shown to illustrate the principal chain length dependence of the UCSTs of the investigated systems. Lines in the picture are given to illustrate trends and to guide the eye.

asymmetry parameter, which yields the scatter of the data in the master plot.

CONCLUSIONS

In this work, we have reported phase diagrams of binary solutions of the ionic liquid C_4mimNTf$_2$ in the *n*-alkyl alcohols C_nOH ($4 < n < 11$) obtained by the synthetic method. The phase diagrams are accurate enough to allow for fits with an approximate scaling relation that presumes Ising critical behavior and takes the asymmetry of the phase diagram into account. The phase diagrams are described by a minimum set of four parameters, which are the critical temperature T_c, the critical mole fraction x_c, the width B, and one parameter A or C for the diameter. In variance to former work,[2,3,26] the assumption of a nonlinear temperature dependence determined by $(T_c - T)^{2\beta}$ with $\beta = {}^1/_3$ does here not lead to an improvement of the representation of the data relative to the assumption of a linear temperature dependence.

As a result of the analysis, we have found that the UCST increases almost linearly with the chain length of the alcohol. Data from other work were included into the analysis and agree nicely with our data, with the exception of the reported work on the octan-1-ol solution. Relative to the critical temperature, all of the other parameters describing the phase diagrams vary little for the different alcohol solutions. The numerical analysis showed that the critical mole fraction and the width increase with the chain length of the alcohol and appear to pass a shallow local maximum. Indications of differences between alcohols with an even or odd number of carbon atoms need to be substantiated. The fits that presume the temperature variation of the diameter with the exponent 2β lead to lower values of the critical mole fraction than those obtained from the fits that presume the rectilinear diameter rule. In former work, the lower value was found to be in better agreement with the experimental figure.[2] The phase diagrams of the solutions of the IL C_4mimNTf$_2$ in alcohols and those of C_{12}mimNTf$_2$ in alcohols become almost identical when expressed in terms of the reduced variables $|T_c - T|/T_c$ and $(x - x_c)/x_c$, which is remarkable because of the rather big changes in the molecular shape and the dielectric permittivity of the solvent. The width of the phase diagrams merges for all systems. Thus, using the theoretically based critical exponents of the phase diagram is advantageous even for data obtained by the cloud-point method, which are limited in their precision.

To put our results in the context of other work where phase diagrams with shorter and longer side chains of $C_x$mimNTf$_2$ were investigated, we show in Figure 6 the critical temperatures determined for our systems together with those from the literature[10,11,14,20,28] and our former reports.[1−3] Figure 6 shows the systematic increase of the UCST with increasing chain length of the alcohol, where the slope decreases with increasing length of the side chain of the IL. The figure includes also the melting temperatures of the pure alcohols.[65] The curves describing the dependence of the critical temperatures of the solutions of the ILs with long side chains on the chain length of the alcohol and the melting temperatures of the alcohols are remarkably similar.

A further elucidation of the critical data and the shapes of the phase diagrams by correlating with other properties such as the dielectric permittivity, the density, and the molecular structure is outside the scope of this work and will be given elsewhere.

AUTHOR INFORMATION

Corresponding Author

*Tel.: +49 421 218 64772. Fax: +49 421 218 64771. E-mail: rathke@uni-bremen.de.

Funding Sources

This work was supported by the German Research Foundation (DFG) within the Priority Program SPP-1191 "Ionic Liquids" (Grants RA 1054/2-2 and SCHR 188/10-1).

ACKNOWLEDGMENT

We thank the colleagues in the Priority Program SPP-1191 for discussions and shared insight.

REFERENCES

(1) Vale, V. R.; Rathke, B.; Will, S.; Schröer, W. Liquid−Liquid Phase Behavior of Solutions of 1-Octyl- and 1-Decyl-3-methylimidazolium Bis(trifluoromethylsulfonyl)imide ($C_{8,10}$mimNTf$_2$) in *n*-Alkyl Alcohols. *J. Chem. Eng. Data* **2010**, *55*, 2030–2038.

(2) Vale, V. R.; Rathke, B.; Will, S.; Schröer, W. Liquid−Liquid Phase Behavior of Solutions of 1-Dodecyl-3-methylimidazolium Bis((trifluoromethyl)sulfonyl)amide (C_{12}mimNTf$_2$) in *n*-Alkyl Alcohols. *J. Chem. Eng. Data* **2010**, *55*, 4195–4205.

(3) Vale, V. R.; Rathke, B.; Will, S.; Schröer, W. Liquid−Liquid Phase Behavior of Solutions of 1-Hexyl-3-methylimidazolium Bis-(trifluoromethylsulfonyl)amide (C_6mimNTf$_2$) in *n*-Alkyl Alcohols. *J. Chem. Eng. Data* **2011**, *56*, 1330–1340.

(4) Wu, C. T.; Marsh, K. N.; Deev, A. V.; Boxall, J. A. Liquid−liquid equilibria of room-temperature ionic liquids and butan-1-ol. *J. Chem. Eng. Data* **2003**, *48*, 486–491.

(5) Marsh, K. N.; Deev, A.; Wu, C. T.; Tran, E.; Klamt, A. K. Room temperature ionic liquids as replacements for conventional solvents: A review. *Korean J. Chem. Eng.* **2002**, *19*, 357–362.

(6) Anthony, J. L.; Maginn, E. J.; Brennecke, J. F. Solution Thermodynamics of Imidazolium-Based Ionic Liquids and Water. *J. Phys. Chem. B* **2001**, *105*, 10942–10949.

(7) Najdanovic-Visak, V.; Esperanca, J. M. S. S.; Rebelo, L. P. N.; Nunes da Ponte, M.; Guedes, H. J. R.; Seddon, K. R.; Szydlowski, J. Phase behaviour of room temperature ionic liquid solutions: An unusually large co-solvent effect in (water + ethanol). *Phys. Chem. Chem. Phys.* **2002**, *4*, 1701–1703.

(8) Najdanovic-Visak, V.; Esperanca, J. M. S. S.; Rebelo, L. P. N.; Nunes da Ponte, M.; Guedes, H. J. R.; Seddon, K. R.; de Sousa, H. C.; Szydlowski, J. Pressure, Isotope, and Water Co-solvent Effects in Liquid−Liquid Equilibria of (Ionic Liquid + Alcohol) Systems. *J. Phys. Chem. B* **2003**, *107*, 12797–12807.

(9) Wagner, M.; Stanga, O.; Schröer, W. Corresponding states analysis of the critical points in binary solutions of room temperature ionic liquids. *Phys. Chem. Chem. Phys.* **2003**, *5*, 3943–3950.

(10) Heintz, A.; Lehmann, J.; Wertz, C. Thermodynamic properties of mixtures containing ionic liquids. 3. Liquid−liquid equilibria of binary mixtures of 1-ethyl-3-methylimidazolium bis(trifluoromethylsulfonyl)imide with propan-1-ol, butan-1-ol, and pentan-1-ol. *J. Chem. Eng. Data* **2003**, *48*, 472–474.

(11) Crosthwaite, J. M.; Aki, S. N. V. K.; Maginn, E. J.; Brennecke, J. F. Liquid phase behavior of imidazolium-based ionic liquids with alcohols. *J. Phys. Chem. B* **2004**, *108*, 5113–5119.

(12) Cerdeirina, C. A.; Troncoso, I.; Ramos, C. P.; Romani, L.; Najdanovic-Visak, V.; Guedes, H. J. R.; Esperanca, J. M. S. S.; Visak, Z. P.; da Ponte, M. N.; Rebelo, L. P. N. Criticality of the $[C_4mim][BF_4]$ + water system. *ACS Symp. Ser.* **2005**, *901*, 175–186.

(13) Heintz, A.; Lehmann, J.; Wertz, C.; Jacquemin, J. Thermodynamic properties of mixtures containing ionic liquids. 4. LLE of binary mixtures of $[C_2MIM][NTf_2]$ with propan-1-ol, butan-1-ol, and pentan-1-ol and $[C_4MIM][NTf_2]$ with cyclohexanol and 1,2-hexanediol including studies of the influence of small amounts of water. *J. Chem. Eng. Data* **2005**, *50*, 956–960.

(14) Crosthwaite, J. M.; Aki, S. N. V. K.; Maginn, E. J.; Brennecke, J. F. Liquid phase behavior of imidazolium-based ionic liquids with alcohols: Effect of hydrogen bonding and non-polar interactions. *Fluid Phase Equilib.* **2005**, *228−229*, 303–309.

(15) Lachwa, J.; Szydlowski, J.; Najdanovic-Visak, V.; Rebelo, L. P. N.; Seddon, K. R.; da Ponte, M. N.; Esperanca, J. M. S. S.; Guedes, H. J. R. Evidence for Lower Critical Solution Behavior in Ionic Liquid Solutions. *J. Am. Chem. Soc.* **2005**, *127*, 6542–6543.

(16) Sahandzhieva, K.; Tuma, D.; Breyer, S.; Kamps, A.; Maurer, G. Liquid−liquid equilibrium in mixtures of the ionic liquid 1-*n*-butyl-3-methylimidazolium hexafluorophosphate and an alkanol. *J. Chem. Eng. Data* **2006**, *51*, 1516–1525.

(17) Saracsan, D.; Rybarsch, C.; Schröer, W. Phase Separation in Solutions of Room Temperature Ionic Liquids in Hydrocarbons. *Z. Phys. Chem.* **2006**, *220*, 1417–1437.

(18) Crosthwaite, J. M.; Muldoon, M. J.; Aki, S. V. N. K.; Maginn, E. J.; Brennecke, J. F. Liquid Phase Behavior of Ionic Liquids with Alcohols: Experimental Studies and Modeling. *J. Phys. Chem. B* **2006**, *110*, 9354–9361.

(19) Lachwa, J.; Szydlowski, J.; Makowska, A.; Seddon, K. R.; Esperanca, J. M. S. S.; Guedes, H. J. R.; Rebelo, L. P. N. Changing from an unusual high-temperature demixing to a UCST-type in mixtures of 1-alkyl-3-methylimidazolium bis{(trifluoromethyl)sulfonyl}amide and arenes. *Green Chem.* **2006**, *8*, 262–267.

(20) Lachwa, J.; Morgado, P.; Esperanca, J. M. S. S.; Guedes, H. J. R.; Canongia Lopes, J. N.; Rebelo, L. P. N. Fluid-Phase Behavior of {1-Hexyl-3-methylimidazolium Bis(trifluoromethylsulfonyl) Imide, $[C_6mim][NTf_2]$, + C_2-C_8 *n*-Alcohol} Mixtures: Liquid−Liquid Equilibrium and Excess Volumes. *J. Chem. Eng. Data* **2006**, *51*, 2215–2221.

(21) Wertz, A.; Lehmann, J. K.; Heintz, A. Liquid−liquid equilibria and liquid−liquid interfacial tension measurements of mixtures containing ionic liquids. *J. Mol. Liq.* **2007**, *131−132*, 2–6.

(22) Domanska, U.; Casas, L. M. Solubility of phosphonium ionic liquid in alcohols, benzene, and alkylbenzenes. *J. Phys. Chem. B* **2007**, *111*, 4109–4115.

(23) Butka, A.; Vale, V. R.; Saracsan, D.; Rybarsch, C.; Weiss, V. C.; Schröer, W. The Liquid− Liquid Phase Transition in Solutions of Ionic liquids with Halide Anions: Criticality and Corresponding States. *Pure Appl. Chem.* **2008**, *80*, 1613–1630.

(24) Domanska, U.; Paduszynski, K. Phase equilibria study in binary systems (tetra-*n*-butylphosphonium tosylate ionic liquid + 1-alcohol, or benzene, or *n*-alkylbenzene). *J. Phys. Chem. B* **2008**, *112*, 11054–11059.

(25) Ferreira, R.; Blesic, M.; Trindade, J.; Marrucho, I.; Canongia-Lopes, J. N.; Rebelo, L. P. N. Solubility of fluorinated compounds in a range of ionic liquids. Cloud-point temperature dependence on composition and pressure. *Green Chem.* **2008**, *10*, 918–928.

(26) Schröer, W.; Vale, V. R. Liquid−liquid phase separation in solutions of ionic liquids: Phase diagrams, corresponding state analysis and comparison with simulations of the primitive model. *J.Phys.: Condens. Matter* **2009**, *21*, No. 424119.

(27) Shiflett, M. B.; Niehaus, A. M. S. Liquid−Liquid Equilibria in Binary Mixtures Containing Substituted Benzenes with Ionic Liquid 1-Ethyl-3-methylimidazolium Bis(trifluoromethylsulfonyl)imide. *J. Chem. Eng. Data* **2010**, *55*, 346–353.

(28) Pereiro, A. B.; Deive, F. J.; Rodriguez, A.; Ruivo, D.; Lopes, J. N. C.; Esperanca, J. M. S. S.; Rebelo, L. P. N. New Insight into Phase Equilibria Involving Imidazolium Bistriflamide Ionic Liquids and their Mixtures with Alcohols and Water. *J. Phys. Chem. B* **2010**, *114*, 8978–8985.

(29) Pitzer, K. S. Critical Phenomena in Ionic Fluids. *Acc. Chem. Res.* **1990**, *23*, 333–338.

(30) Weingärtner, H.; Schröer, W. Criticality of Ionic Fluids. *Adv. Chem. Phys.* **2001**, *116*, 1–66.

(31) Wiegand, S.; Briggs, M. E.; Levelt Sengers, J. M. H.; Kleemeier, M.; Schröer, W. Turbidity, light scattering, and coexistence curve data for the ionic binary mixture triethyl *n*-hexyl ammonium triethyl *n*-hexyl borate in diphenyl ether. *J. Chem. Phys.* **1998**, *109*, 9038–9051.

(32) Kleemeier, M.; Wiegand, S.; Schröer, W.; Weingärtner, H. The liquid−liquid phase transition in ionic solution: Coexistence curves of tetra-*n*-butylammonium picrate in alkyl alcohols. *J. Chem. Phys.* **1999**, *110*, 3085–3099.

(33) Oleinikova, A.; Bonetti, M. Coexistence curve of the ionic binary mixture tetra-*n*-butylammonium picrate in 1-dodecanol. *Chem. Phys. Lett.* **1999**, *299*, 417–422.

(34) Schröer, W.; Wiegand, S.; Weingärtner, H. The effect of short-range hydrogen-bonded interactions on the nature of the critical point of ionic fluids. Part II: Static and dynamic light scattering on solutions of ethylammonium nitrate in *n*-octanol. *Ber. Bunsen-Ges. Phys. Chem.* **1993**, *97*, 975–982.

(35) Barthel, J.; Carl, E.; Gores, H. J. Coulombic liquid−liquid phase separation of dilithium hexafluoropropane-1,3-bis[sulfonylbis(trifluoromethylsulfonyl)methanide] solutions in diethyl carbonate. *Electrochem. Solid State Lett.* **1999**, *2*, 218–221.

(36) (a) Reid, R. C.; Prausnitz, J. M.; Sherwood, T. K. *The Properties of Gases and Liquids*, 3rd ed.; McGraw Hill: New York, 1977. (b) Poling, B.; Prausnitz, J. M.; O'Connell, J. P. *The Properties of Gases and Liquids*, 5th ed.; McGraw Hill: New York, 2001.

(37) Poole, C. F.; Poole, S. K. Extraction of organic compounds with room temperature ionic liquids. *J. Chromatogr., A* **2010**, *1217*, 2268–2286.

(38) *Ionic Liquids in Synthesis*, 2nd ed.; Wasserscheid, P., Welton, T., Eds.; Wiley-VCH: Weinheim, Germany, 2008.

(39) Wagner, M.; Stanga, O.; Schröer, W. The liquid−liquid coexistence of binary mixtures of the room temperature ionic liquid 1-methyl-3-hexylimidazolium tetrafluoroborate with alcohols. *Phys. Chem. Chem. Phys.* **2004**, *6*, 4421–4431.

(40) Huddlestone, J. G.; Visser, A. E.; Reichert, W. M.; Willauer, H. D.; Broker, G. A.; Rogers, R. D. Characterization and comparison of hydrophilic and hydrophobic room temperature ionic liquids incorporating the imidazolium cation. *Green Chem.* **2001**, *3*, 156–164.

(41) Swatloski, R. P.; Holbrey, J. D.; Rogers, R. D. Ionic liquids are not always green: Hydrolysis of 1-butyl-3-methylimidazolium hexafluorophosphate. *Green Chem.* **2003**, *5*, 361–363.

(42) Ferreira, A. R.; Freire, M. G.; Ribeiro, J. C.; Lopes, F. M.; Crespo, J. G.; Coutinho, J. A. P. An Overview of the Liquid−-Liquid

Equilibria of (Ionic Liquid + Hydrocarbon) Binary Systems and Their Modeling by the Conductor-like Screening Model for Real Solvents. *Ind. Eng. Chem. Res.* **2011**, *50*, 5279–5294.

(43) Canongia Lopes, J. N. A.; Pádua, A. A. H. Nanostructural Organization in Ionic Liquids. *J. Phys. Chem. B* **2006**, *110*, 3330–3335.

(44) Costa Gomes, M. F.; Canongia Lopes, J. N.; Pádua, A. A. H. Thermodynamics and Heterogeneity of Ionic Liquids. *Top. Curr. Chem.* **2009**, *290*, 161–183.

(45) Triolo, A.; Mandanici, A.; Russina, O.; Rodrguez-Mora, V.; Cutroni, M.; Hardacre, C.; Nieuwenhuyzen, M.; Bleif, H.-J.; Keller, L.; Ramos, M. A. Thermodynamics, Structure, and Dynamics in Room Temperature Ionic Liquids: The Case of 1-Butyl-3-methyl Imidazolium Hexafluorophosphate ([bmim][PF_6]). *J. Phys. Chem. B* **2006**, *110*, 21357–21364.

(46) Triolo, A.; Russina, O.; Bleif, H.; Cola, E. D. Nanoscale segregation in room temperature ionic liquids. *J. Phys. Chem. B* **2007**, *111*, 4641–4644.

(47) Bradley, A. E.; Hardacre, C.; Holbrey, J. D.; Johnston, S.; McMath, S. E. J.; Nieuwenhuyzen, M. Small-Angle X-ray Scattering Studies of Liquid Crystalline 1-Alkyl-3-methylimidazolium Salts. *Chem. Mater.* **2002**, *14*, 629–635.

(48) Holbrey, J. D.; Reichert, W. M.; Rogers, R. D. Crystal structures of imidazolium bis(trifluoromethansulfonyl)imide ionic liquid salts: the first organic salt with a *cis*-TFSI anion conformation. *Dalton Trans.* **2004**, 2267–2271.

(49) Domb, C. *The Critical Point*; Taylor and Francis: London, 1996.

(50) Ivanov, D. Y. *Critical Behavior of Non-Ideal Systems*; Wiley-VCH: Weinheim, Germany, 2008.

(51) Rowlinson, J. S.; Swinton, F. L. *Liquids and Liquid Mixtures*, 3rd ed.; Butterworths: London, 1982.

(52) Marsh, K. N. Thermodynamic Properties of Organic Compounds and their Mixtures: Densities. *Landolt Börnstein, Numerical Data and Functional Relationships in Science and Technology: New Series IV/8B-J*; Springer: Berlin, 1996−2003.

(53) Kayser, R. F.; Raveche, H. J. Asymptotic density correlations and corrections to scaling for fluids with non-finite-range interactions. *Phys. Rev. A* **1984**, *29*, 1013–1015.

(54) Schröer, W. *Criticality of Ionic Liquids in Solution*; Henderson, D., Holovko, M., Trokhymchuk, A., Eds.; Ionic Matter: Modern Trends in Theory and Applications; NATO Science Series, Vol. 206; Springer: Dordrecht, 2005; pp 143−180.

(55) Levelt Sengers, J. M. H.; Harvey, A. H.; Wiegand, S. In *Equations of State for Fluids and Fluide Mixtures*; Sengers, J. V., Kayser, R. F., Peters, C. J., White, H. J., Eds.; Elsevier: Amsterdam, 2000; p 805.

(56) Kim, Y. C.; Fisher, M. E.; Orkoulas, G. Asymmetric fluid criticality I. Scaling with pressure mixing. *Phys. Rev. E* **2003**, *67*, No. 061506.

(57) Wang, J.; Anisimov, M. A. Nature of vapor−liquid asymmetry in fluid criticality. *Phys. Rev. E* **2007**, *75*, No. 051107.

(58) Wang, J.; Cenderina, C. A.; Anisimov, M. A.; Sengers, J. V. Principle of isomorphism and complete scaling for binary-fluid criticality. *Phys. Rev E.* **2008**, *77*, No. 031127.

(59) Pérez-Sánchez, G.; Losada-Pérez, P.; Cerdeiriña, C. A.; Sengers, J. V.; Anisimov, M. A. Asymmetric criticality in weakly compressible liquid mixtures. *J. Chem. Phys.* **2010**, *132*, No. 154502.

(60) Behnejad, H.; Sengers, J. V.; Anisimov, M. A. Thermodynamic Behaviour of Fluids near Critical Points. In *Applied Thermodynamics of Fluids*; Goodwin, A. R. H., Sengers, J. V., Peters, C. J., Eds.; RSC Publishing: Cambridge, U.K., 2010; pp 321−367.

(61) Wohlfarth, C. Static Dielectric Constants of Pure Liquids and Binary Liquid Mixtures. *Landolt Börnstein, Numerical Data and Functional Relationships in Science and Technology: New Series IV/6*; Springer: Berlin, 1991.

(62) Guggenheim, E. A. The Principle of Corresponding States. *J. Chem. Phys.* **1945**, *13*, 253–261.

(63) Schröer, W. Universality and Corresponding State Behaviour in the Phase Diagrams of Alcohol Solutions of Ionic Liquids with the BF_4^- Anion. *J. Mol. Liq.* **2006**, *125*, 164–173.

(64) Dittmar, H.; Butka, A.; Vale, V. R.; Schröer, W. Liquid−liquid phase transition in the ionic solutions of tetra-*n*-butylammonium chloride in *o*-xylene and ethylbenzene: Phase diagrams and corresponding state analysis. *J. Mol. Liq.* **2009**, *145*, 116–128.

(65) *Handbook of Chemistry and Physics*, 76th ed.; Lide, D. R., Ed.; CRC Press: Boca Raton, FL, 1995.